Materials Today Bio 32 (2025) 101774

Contents lists available at ScienceDirect

Materials Today Bio

journal homepage: www.journals.elsevier.com/materials-today-bio

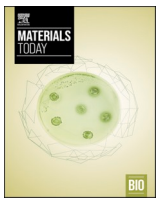

Targeted self-assembled anti-NFκB AuNCs-aptamer nanoplatform for precise theranostics via tailored follicle regeneration

Xiangdong Lai [a], Xiaoyang Zhang [a], Jiejuan Lai [b], Weiwei Zhao [c], Zhongquan Song [d], Yuanyuan Chen [a], Miraj Ud din [a], Muhammad Faizan Munawer [a], Hui Jiang [a,*], Xiaohui Liu [a,**], Xuemei Wang [a,***]

[a] State Key Laboratory of Digital Medical Engineering, School of Biological Science and Medical Engineering, Southeast University, Nanjing, 210096, China
[b] Department of Hepatobiliary Surgery, Southwest Hospital, Third Military Medical University (Army Medical University), Chongqing, 400038, China
[c] State Key Laboratory Breeding Base for The Protection and Utilization of Biological Resources in Tarim Basin, College of Life Science and Technology, Tarim University, Alar, Xinjiang, 843300, China
[d] Department of Pulmonary and Critical Care Medicine, Zhongda Hospital, Medical School, Southeast University, Nanjing, 210009, China

ARTICLE INFO

Keywords:
anti-NFκB aptamer
Oxidative stress microenvironment
Self-assembly
AuNCs-Aptamer
Hypertrichosis

ABSTRACT

NFκB is a vital transcription factor for the regulation of hair follicle cycle. As a therapeutic target, NFκB is specifically blocked by RNA aptamer with negligible side effects, but the targeted transmembrane transport of anti-NFκB aptamer remains a challenge due to its negative charge under physiological conditions. In this study, taking advantage of the depilation-induced oxidative stress microenvironment (OSM), it was confirmed for the first time that self-assembled gold nanoclusters and aptamer (AuNCs-Aptamer) complexes formed in the skin and enhanced the therapeutic effect of anti-NFκB aptamer drugs, effectively blocking the NFκB-mediated inflammatory response and inhibiting hair follicle regeneration. The hematoxylin-eosin (HE) staining of tissue section and hematology analysis demonstrated that OSM-responsive self-assembled AuNCs-Aptamer caused no toxicity to the living organism. Moreover, self-assembly occurred only in the oxidative stress-injured skin cells rather than the normal cells, which revealed that this self-assembly was a targeted, safe and effective therapy for hypertrichosis.

1. Introduction

Hair follicles are important epidermal accessories that produce hairs [1–5]. Throughout one's life, the inferior part of the hair follicle periodically degenerates, shortens and is rebuilt to control the orderly growth of hair [6–9], corresponding to the three different stages of hair follicle cycle (catagen, telogen and anagen), respectively. The skin injury from the skin care products, drugs and ultraviolet radiation is usually accompanied by the overproduction of reactive oxygen species (ROS) [10–12] and causes the hypertrichosis [13–17]. This kind of skin disease aesthetically loses its original beauty and even causes some serious spiritual and psychological problems such as anxiety, inferiority and irritability to the patients. ROS transmit biological signals as second messengers, activate the proliferation and differentiation of hair follicle stem cells (HFSCs) and promote the transformation of the hair follicle cycle from telogen into anagen [18–23]. Corticosteroid addictive dermatitis caused by abuse of hormone-containing skin care products are accompanied by oxidative stress from excess ROS, leading to hypertrichosis [24–26]. Minoxidil, a low dose oral drug for alopecia, causes the side effect such as dermatitis and hypertrichosis [27–29]. The dermatomyositis is characterized by inflammation of muscles and skin along with rare hypertrichosis [30,31]. The omeprazole causes generalized hypertrichosis by increasing the levels of mediator of inflammation prostaglandin E_2 [32]. Vorasidenib [33] and consecutive cetuximab [34] administration causes the exaggerated side effect of hairy skin. Because limited therapies are available and often unsatisfactory, patients are usually under psychological distress [35–37]. Current pharmacological therapy, like eflornithine, presents the serious adverse

This article is part of a special issue entitled: Biomarker published in Materials Today Bio.

* Corresponding author.
** Corresponding author.
*** Corresponding author.
E-mail addresses: sungi@seu.edu.cn (H. Jiang), 101013182@seu.edu.cn (X. Liu), xuewang@seu.edu.cn (X. Wang).

https://doi.org/10.1016/j.mtbio.2025.101774
Received 10 February 2025; Received in revised form 12 April 2025; Accepted 16 April 2025
Available online 17 April 2025

effects, and clinical efficacy is not ideal [37–39]. Undesired hair removal by means of physiotherapy (photoepilation and electrolysis) is painful and repeated [40], destroys the hair follicles [41] and ablates cutaneous stem cell reservoir, which is not good for wound healing [42–47]. Therefore, it is necessary to develop a safe and effective strategy for treating hypertrichosis (see Scheme 1).

NFκB is involved in the regulation of mouse hair follicle cycle as an essential transcription factor for the activation, maintenance and growth of HFSCs [48–50]. Therefore, NFκB can be used as a therapeutic target. The aptamer, a short single-stranded DNA or RNA with unique 3D structure, is a promising therapeutic against a wide variety of disorders attributing to its protein-binding ability, the selective limitation on protein activity with negligible side effects [51], the easy synthesis and modification at large scale and low price, the rapid penetration into tissues and the low immunogenicity to the body [52]. However, the transmembrane delivery of therapeutic aptamers against the intracellular targets remains a challenge. The retroviral vectors are used to generate therapeutic anti-NFκB aptamers directly inside cells, which has biosafety concerns [53–55]. The poor uptake of the anti-NFκB aptamers into mammalian cells results in high dosage and repeated administrations, which is hard to achieve a significant therapeutic effect [56,57]. The main reason is that nucleic acids are negatively charged under physiological conditions.

The positively charged metal ions not only easily interact with the negatively charged phosphate backbone through the simple electrostatic attraction, but also accept electrons from the nucleobase units or the phosphatic oxygen to form coordination complexes [58]. Due to very stable chemical properties, good biocompatibility and intrinsic optical characteristics, gold ion and gold nanoclusters have a wide range of biomedical applications [59–62]. Therefore, we hypothesized that $HAuCl_4$ could be self-assembled with aptamers into the complexes to facilitate the targeted transmembrane delivery of the aptamer drugs into the oxidative stress-damaged hair follicle cells. For proof of the concept, the anti-NFκB/p50 aptamer was used to form a coordination precursor complex with $HAuCl_4$ for investigating its effect on hair follicle regeneration. In this study, for the first time, AuNCs-Aptamer complexes were self-assembled in depilation-induced skin trauma microenvironment. Moreover, this self-assembly occurred only in the oxidative stress-injured skin cells rather than the normal cells, effectively blocking the nuclear transcription factor kappa B (NFκB)-mediated inflammatory response signal pathway and inhibiting hair follicle regeneration. Therefore, it is a targeted, safe and effective strategy for delivering functional aptamers and treating hypertrichosis.

2. Materials and methods

2.1. Synthesis of anti-NFκB aptamer

The optimized aptamer against murine NFκB/p50 by truncation was adopted from Huang et al. [63], and the 29-nt p50 RNA aptamer (5-CAUACU$_2$GA$_3$CUGUA$_2$G$_2$U$_2$G$_2$CGUAUG-3) was custom-synthesized as a phosphorothioate backbone form [64–66] by Sangon Biotech (Shanghai, China), in which a nonbridging oxygen atom of the phosphate was displaced with sulfur atom to enhance the biological stability of aptamer against nuclease [66–68].

2.2. Depilation-induced trauma model

All the animal experiments were allowed by Animal Care Research Advisory Committee of Southeast University. All the experiment procedures related to animal were conducted under the approval of the Animal Research Ethics Board of Southeast University. Referring to our previous experiment procedure [69], we established hair plucking-trauma model in C57BL/6 mice. In short, mouse hair follicles stayed quiescent after postnatal 7–8 weeks, and the hair was plucked by rosin/wax melt. Half an hour after mice were depilated, they were divided into the five different groups as follows. 1 mM $HAuCl_4$ solution (25 μL, pH = 7), 0.5 mM $HAuCl_4$ solution (25 μL, pH = 7), PBS (25 μL), 10 μM Aptamer (25 μL), and 25 μL Au + Apt precursors (1 mM $HAuCl_4$ +10 μM Aptamer) were intradermally injected, respectively (n = 6 each group). It was eligible to inject drugs into the superficial part of the skin with 40-unit insulin syringes and form a skin protrusion temporarily. Be careful not to inject drugs into the subcutaneous tissue. Mice were administered once a day for three consecutive days, and each mouse was kept in a specific pathogen-free grade environment and in the separate cage to avoid the skin being scratched and broken. The intradermal drug injection is a common method in the research field of hair follicle as an essential accessory of the epidermis [70–78], especially in the beauty field [73,79]. The technical term is “mesotherapy technique” by which low doses of therapeutic agents and bioactive substances are administered by intradermal injections to the skin [80]. Moreover, we adopted 30-gauge needles (0.3 mm × 8 mm) for injection, which was thinner and

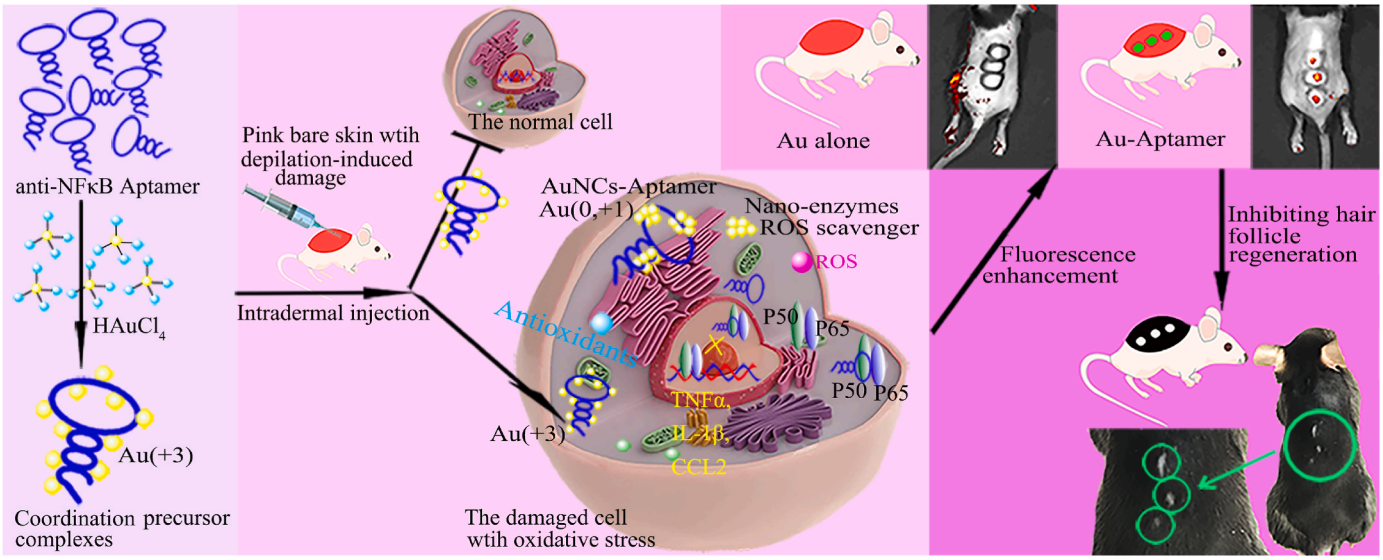

Scheme 1. Schematic diagram of self-assembled AuNCs-Aptamer in the depilation-induced injured skin after the administration of the aptamer and $HAuCl_4$ coordination precursor complexes, and AuNCs-Aptamer inhibiting hair follicle regeneration by negatively regulating the NFκB(p50/p65)-mediated inflammatory response.

safer than that the literature recommended [81].

2.3. Fluorescence imaging for the small animal

For *in vivo* fluorescence imaging, mice were successfully pre-anesthetized by 4 % isoflurane gas and wore the masks for continuous inhalation of 2 % isoflurane to maintain anesthesia. Fluorescence pictures were taken by the fluorescence imager for live small animals (Perkin Elmer, IVIS Lumina XRMS Series III) under 480 nm excitation.

2.4. Cell viability assay by cell counting kit 8 (CCK-8)

Commercialized JB6 (resistant to the promotion of transformation by phorbol esters) is an immortalized mouse epithelial cell line. According to the manufacturer's instructions, the cell viability was tested for three times via CCK-8 (Beyotime, Shanghai, China). JB6 cells in the exponential growth were inoculated into 96-well plates with 5000 cells per well. After adequate adhesion, the cells were treated with $HAuCl_4$ solution (pH = 7) for 24 h. 10 μL of CCK-8 solution was added into each well. After incubating in the cell incubator for 3 h, the absorbance value of the reaction product was read at 450 nm via a full wavelength microplate reader.

2.5. Detection of intracellular AuNCs-aptamer after scratch injury

JB6 cells were inoculated in the laser confocal culture dishes at a density of 5×10^5 cells per dish and grew in the cell incubator overnight. Cells were treated with PBS, $HAuCl_4$ solution (Au, pH = 7), anti-NFκB aptamer (Apt), and $HAuCl_4$ + anti-NFκB aptamer (Au + Apt), respectively, and 10 μL tips were used to scratch the cells to induce cell injury. After another 8 h incubation, the fluorescence was observed, and the pictures were taken by laser confocal microscopy at 488 nm excitation.

2.6. The extraction of AuNCs-aptamer

After the mice were euthanatized, the drug-administrated skin was harvested and homogenized fully using the glass tissue homogenizer. The homogenate was frozen in the liquid nitrogen for 5 h and then fully thawed in the 37 °C water bath repetitively for more than six times to break the cell membranes completely. After centrifugation at 3500 rpm for 5 min, the supernatant was acquired and lyophilized for characterization.

2.7. The characterization of AuNCs-aptamer

For high resolution transmission electron microscope imaging (HR-TEM) by Talos F200X G2, the extracted sample was dropped on carbon-coated copper grid (Electron Microscopy Sciences). For energy dispersive spectrometer (EDS) and element mapping, the extracted sample was dripped on the carbon-coated copper grid and dried with infrared heater for 10 min. For X-ray photoelectron spectroscopy (XPS), the lyophilized sample was compensated for charging with a low-energy electron beam and analyzed by PHI Quantera II using Al Kα radiation (hv = 1486.6 eV). The peak of C1s (binding energy = 284.4 eV) was applied to correct the sample charging. For atomic force microscope (AFM) imaging, samples diluted with deionized water were deposited onto silicon wafer carriers with oxide layer and imaged using NanoWizard® 4 XP BioScience atomic force microscope.

2.8. Hematoxylin and eosin staining (HE)

The skin tissue slides were dewaxed twice in the pure xylene, hydrated in graded alcohols and rinsed gently with running tap water for 4 min. The sections were stained at first with the hematoxylin solution for 1 min. Subsequently, the sections were rinsed gently with running tap water for 3 min. After nuclear staining was adjusted by hydrochloric acid ethanol solution, sections were counterstained with eosin for 15 s and immediately rinsed with running tap water. The tissue slides were dehydrated by reverse gradient alcohol and mounted with neutral resin for observation under a microscope.

2.9. Detection of cyanine 3 (Cy3)-labeled aptamer after scratch injury

JB6 cells were inoculated in the sterile petri dishes at a density of 10^6 cells per dish at 37 °C overnight. After 10 μL tips were used to scratch the cells to induce cell injury, cells were treated with PBS, $HAuCl_4$ solution (pH = 7), Cy3-labeled anti-NFκB aptamers (Cy3Apt), and $HAuCl_4$ + Cy3Apt (Au + Cy3Apt), respectively. After 8 h incubation, the red fluorescence was detected by fluorescence microscopy at 550 nm excitation.

2.10. Biostability assay of aptamers

Synthetic aptamers (5 μM) were incubated in mouse serum at 37 °C. Samples were acquired at different time points (0, 1, 6, 12, 18, 24 h) and electrophoresed in a 3 % agarose gel. Residual aptamer products were semi-quantitatively analyzed by Image J software (%).

2.11. Affinity and specificity of aptamer binding to NFκB/p50

The affinity and specificity of aptamer binding to target were determinated by enzyme-linked oligonucleotide assay (ELONA). 96-well polystyrene microtiter plates with high adsorption ability were coated with 300 ng per well of recombinant p50 protein (residues 39–364, ordered from Sino Biological, Inc. China) in 100 μL of carbonate solution at 4 °C overnight. After discarding the coating solution, the plate wells were washed three times with 10 mM HEPES buffer (pH = 7.5) to eliminate any unbound protein and blocked with 100 μL per well of HEPES containing 5 % bovine serum albumin (HEPESB) for 40 min at RT. Afterwards, biotin-labeled aptamers were diluted in binding buffer (HEPES and 0.1 M NaCl) at different concentrations (0 nM, 5 nM, 15 nM, 45 nM, 135 nM, and 405 nM), denatured at 95 °C for 10 min and cooled on ice for 10 min. Next, 100 μL of the aptamer solution were supplemented to each well, and the reaction mixture was incubated for 1 h at 37 °C. The microplate wells were washed again four times with HEPES containing 0.005 % tween 20 (HEPEST) to remove unbound aptamers, and the bound aptamers in each well were detected using 100 μL of a 1/1000 dilution of streptavidin-conjugated horseradish peroxidase in HEPESB. After 1-h incubation on a shaker at 37 °C, the plate wells were washed four times with HEPEST to eliminate any unbound materials. The color developing reaction was carried out by tetramethylbenzidine kit following the manufacturer's instruction. The data were obtained in triplicates per each aptamer concentration in all cases. The K_D values of the aptamers were obtained by the absorbance values corresponding to a series of different concentration of aptamers fitted into the curve equation $Y = V_{max} * X/(K_m + X)$ through the statistics software Origin 2023. Mitogen-activated protein kinase 1 (MAPK1/ERK2), mitogen-activated protein kinase 8 (MAPK8/JNK1), SARS-CoV-2 spike subunit-1 (S1), angiotensin-converting enzyme 2 (ACE2), and programmed cell death ligand 1 (PDL1) protein were used as controls in the specificity assay. The MAPK1, MAPK8, ACE2 protein were bought from Sino Biological, Inc. China. The S1 and PDL1 proteins were purchased from ACRO Biosystems, Beijing, China.

2.12. Enzyme-linked immunosorbent assay (ELISA)

The mouse dorsal skin tissues were homogenized, and the tissue homogenate was cryogenically centrifuged at 13000 g for 8 min to acquire the supernatant for detection. The total protein concentration of each sample was measured by the enhanced BCA Protein Assay Kit (Beyotime, Shanghai, China). Following the manufacturer's product instruction in ELISA kit, the absorbance of each sample was detected at

450 nm wavelength, and the concentration of the interested protein factors in the tested specimen was calculated by standard curve equation. The result was expressed as the amount of the interested protein factor contained in total skin protein (pg/mg).

2.13. Immunofluorescence staining

The dorsal skins from each group of mice were embedded in the paraffin wax for the tissue section. Subsequently, the skin tissue sections were dewaxed, rehydrated and heated in microwave for antigen repair. After blocking antigen with 5 % BSA, the primary antibodies against nuclear-associated antigen (Ki67), pan-cytokeratin (AE13) and trichohyalin (AE15) were diluted in a ratio of 1:100 (Santa Cruz Biotechnology, Shanghai Co., Ltd.) to incubate with the samples, respectively. The Cy3-labeled secondary antibody (Beyotime, Shanghai, China) was diluted in a ratio of 1:100 to bind to the primary antibody. The cell nucleuses were counterstained for 10 min with 4′, 6-diamidino-2-phenylindole (DAPI, Beyotime, Shanghai, China).

3. Results and discussion

3.1. Self-assembled AuNCs-aptamer inhibiting hair follicle regeneration

When the dose concentration of $HAuCl_4$ precursors was 1 mM or 0.5 mM, no obvious fluorescence was observed (Fig. S1). When the concentration of $HAuCl_4$ was higher than 1 mM, it led to more toxicity.

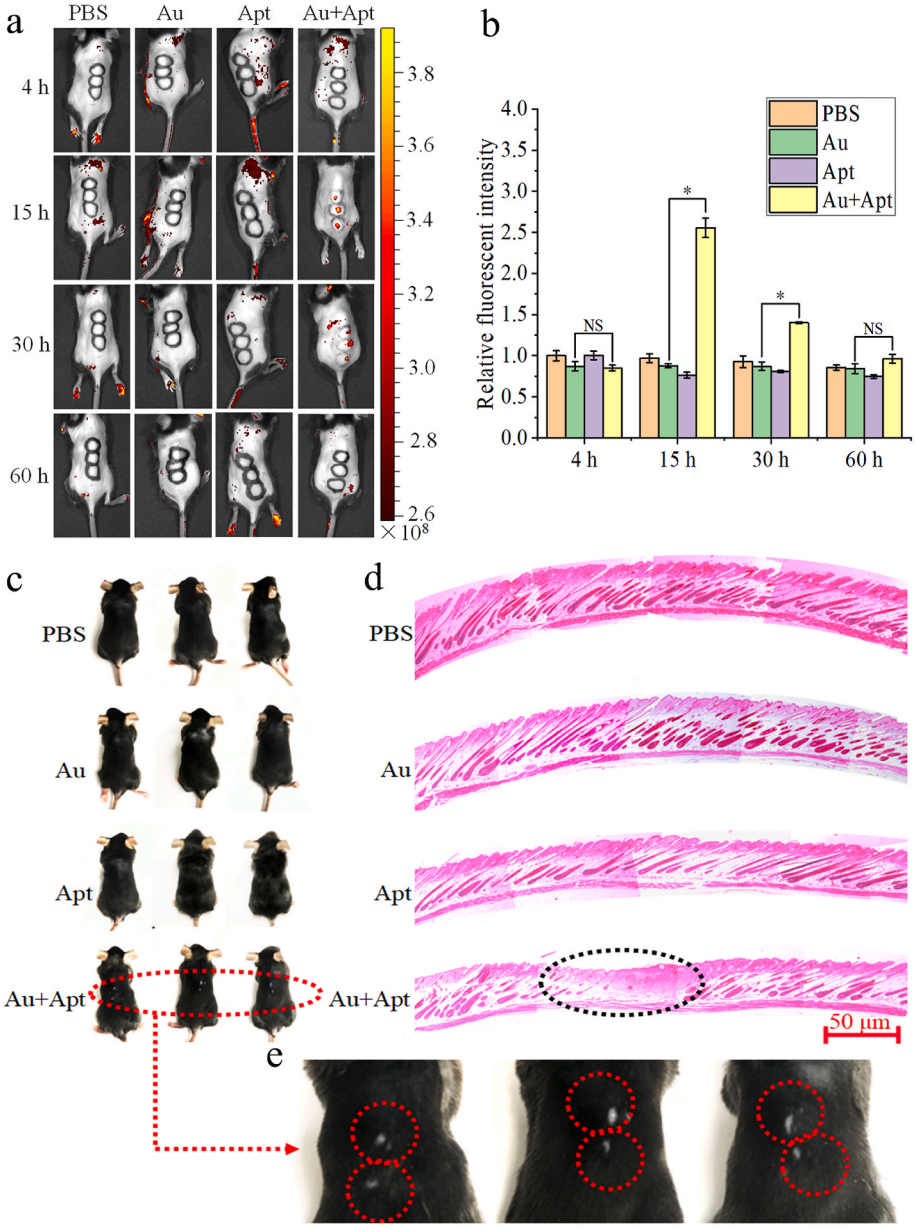

Fig. 1. (a) *In vivo* fluorescence imaging at the different time points after the first administration. (b) The right histogram showed the quantitative analysis statistics of the relative fluorescence signal intensity in the drug-administrated skin sites from 4 different groups of PBS, Au, Apt, and Au + Apt. The unit of average radiant efficiency was $[p/s/cm^2/sr]/[\mu W/cm^2] \times 10^8$. The fluorescence signal intensity of the dorsal skin at the dosed site from PBS group mice at 4 h was standardized to 1. (*$P < 0.05$, and NS: no significance). (c) Camera photographs of PBS, Au, Apt and Au + Apt group mice on the 10^{th} day post the first dose. (d) HE staining of the skin tissue sections from PBS, Au, Apt and Au + Apt group mice on the 10^{th} day post the first dose. The dashed circle indicated the site of dose and supression of the hair follicle regeneration. The HE staining image of each group was made up of the four or five photos taken in succession and connected by front and back. (e) Local magnified picture of the dorsal skin of Au + Apt group mice.

When the concentration of $HAuCl_4$ was lower than 1 mM, such as 0.5 mM, it had poor delivery effect, resulting in no hair inhibition (Fig. S2). The particle size below the renal clearance threshold (about 5.5 nm) favoured renal filtration and excretion and was safe for organisms [82]. Therefore, for biosafety and delivery effect, the low concentration of $HAuCl_4$ (1 mM) for injection was appropriate in our experiments, and exhibited a good effect of hair inhibition (Fig. 1). Considering both biosafety and effectiveness of the aptamer delivery, 1 mM $HAuCl_4$ and 10 μM aptamer (Au + Apt) coordination precursors were injected into the dorsal skin with the depilation-induced trauma to investigate the response of Au + Apt coordination precursors to the OSM and its effect on hair regeneration (Fig. S3). At the different time points of post-administration, the mice were anesthetized with 2 % isoflurane gas, and the fluorescence pictures were taken by in *vivo* fluorescence imager under 480 nm excitation. As shown in Fig. 1a and b, the fluorescence signals of the dorsal skin at the administration site among PBS, Au and Apt group mice exhibited no significant difference. The dorsal skin at the injection site in Au + Apt group mice showed the obviously strengthened fluorescence signal at 15 h, compared to those in PBS, Au and Apt groups of mice. Subsequently, the fluorescence signals of the dorsal skin in the Au + Apt group mice decreased gradually from 30 h to 60 h. Above results suggested that the OSM-responsively self-assembled AuNCs-Aptamer complexes were synthesized successfully. There was no obvious fluorescence after administration of the $HAuCl_4$ alone, while the fluorescence was significantly enhanced after the injection of Au + Apt precursors, which could be explained by aggregation-induced fluorescence emission [83,84]. 60 h after the first dose, the mice were euthanatized, and the main organs were collected for *ex vivo* fluorescence imaging. No apparent differences in fluorescence signals were found in the main organs among all groups of mice (Fig. S4), which indicated AuNCs-Aptamer complexes were not accumulative in the internal organ and safe for the body. We had the similar results in imaging of JB6 cells with scratch-induced injury. Firstly, according to CCK-8 assays, there was no obvious cytotoxicity after treatment with different concentration of $HAuCl_4$ from 10 μmol/L to 175 μmol/L (Fig. S5). Subsequently, we chose 10 μmol/L $HAuCl_4$ solution for the following cell scratch injury experiment and found that the damaged cell along the scratch in Au + Apt group showed stronger fluorescence signals than that in Au group (Fig. S6), which further indicated the effect of fluorescence enhancement as the same as *in vivo* imaging after the formation of the oxidative stress-responsively self-assembled AuNCs-Aptamer. Gold interacted with the sulfur atoms [85], nitrogen atoms [86,87] and hydroxyl groups [151] in the phosphorothioated nucleic acid, which provided an ideal template for reducing Au^{+3} to AuNCs (0/+1) under OSM [88–90].

Before functional validation of the aptamer, the serum stability of phosphorothioated aptamers was demonstrated to be good and met the requirements of *in vivo* use. Natural nucleic acid aptamers were susceptible to *exo*- and *endo*-nucleases and rapidly degraded *in vivo* through the hydrolysis of phosphodiester bonds [91], and the half-time in human blood was only a few minutes [92,93]. The phosphorothioate, in which non-bridging oxygen atoms in the phosphate skeleton were replaced by sulfur, was a common strategy for improving resistance to nuclease [66,68,94] without impeding or even enhancing affinity [95,96]. Therefore, prior to functional validation of the aptamer, it was demonstrated that the serum stability of phosphorothioated aptamers was good and met the requirements of *in vivo* use (Fig. S7). Meanwhile, the aptamer still maintained its high affinity at the nanomolar level (4.82 ± 0.37 nM) and good specificity (Fig. S8). 10 days after the first intradermal administration, the dorsal skin injected with Au + Apt exhibited the inhibition of hair regeneration. However, the dorsal skins injected with PBS, Au and Apt respectively grew black, and the hair grew (Fig. 1c, d and 1e). A single targeted site was injected once a day for three times. The hair follicles on both sides of a single injection targeted site stayed in the typical anagen phase, and their growth was not inhibited, indicating that there was no influence between different injection targeted sites. Therefore, only a single targeted site was injected for efficacy. 10 days after depilation, HE staining of the main internal organs demonstrated that the AuNCs-Aptamer caused no toxicity (Fig. S9). To further evaluate the biosafety of the AuNCs-Aptamer, the blood was acquired for the hematology test after euthanizing the mice. The routine blood examinations indicated that the cell counting of erythrocytes, leukocytes, or platelets among all groups of mice showed no significant difference (Table S1). The serum biochemical parameters, including the renal function indexes (urea and creatinine), the liver function indexes (aspartate transaminase and alanine transaminase), and the cardiac function index (creatine kinase), were in the normal range, and the self-assembled AuNCs-Aptamer did not cause damage to the kidney, liver and heart (Table S2). By and large, above results revealed that the AuNCs-Aptamer was a safe and effective therapeutic for inhibiting hair follicle regeneration.

3.2. Characterizing the AuNCs-aptamer

To provide further evidence on the self-assembled AuNCs-Aptamer, the skin extract was used for the characterization as follows. 12 h after the first drug-administration, AuNCs-Aptamer in the injected skin site were extracted by the repeated freeze-thaw method. The typical HR-TEM images (Fig. 2a and b) and the statistical histogram of particle size distribution **(the insert of** Fig. 2a) revealed that AuNCs had a very concentrated diameter distribution in the 1.8–2.6 nm range. The average particle size (2.18 nm) was below the renal clearance threshold (about 5.5 nm), favouring renal filtration and excretion and reducing the organ toxicity [82]. From the analysis of HR-TEM, the interplanar crystal spacing was 0.22 nm, corresponding to the Au (111) plane **(the insert of** Fig. 2b). Dark-field scanning transmission electron microscopy and elemental mapping demonstrated that Au, C, N, and O elements were uniformly distributed in the skin extract (Fig. S10). XPS testified that four peaks coincided with the emission of 4f photoelectrons from Au^0 and Au^{+1} (Fig. 2c). After calculating the integrated peak area, the atomic percentages of Au^0 and Au^{+1} co-existing in the skin extract were 62.8 % and 37.2 %, respectively. Under oxidative stress, total antioxidants were increased to maintain cell homeostasis [97–99], which provided the favorable conditions for the reduction of Au^{+3} to Au^0 and Au^{+1}. EDS analysis further demonstrated that gold primitive element and the organic component were present in the skin extract. However, the proportion of gold primitive element in the skin extract was relatively low due to the formation of AuNCs-Aptamer (Fig. 2d and Table S3). In the AuNCs-Aptamer, there were a large amount of RNA aptamers on the surface of the complexes, which would reduce the amount of gold exposed to surface. Positively charged mono-valent gold Au^{+1} facilitated binding between AuNCs and aptamer through electrostatic interactions. Furthermore, the phosphorothioate backbone modification provided a stronger anchoring point for AuNCs through the sulfur atom compared to oxygen atoms on phosphate groups [85]. In addition to the phosphate groups, the various other functional units (hydroxyl groups on the deoxyribose moieties and nitrogen atoms on the bases) in nucleic acid specifically interacted with a gold or gold ion [151], which made nucleic acid an ideal template for synthesizing metal nanoclusters [88–90]. Meanwhile, some studies revealed metal nanoclusters bound to N_3 atoms of cytosine [86], and gold nanoparticles bound to guanine through the non-bonding interaction [87]. Because the high energy electron beam from TEM might destroy the three-dimensional conformation of the AuNCs-Aptamer, especially the structure of the nucleic acid aptamer in the complexes, it was necessary to further characterize the complexes by atomic force microscopy (AFM). According to the AFM height profiles (Fig. 2e–k), it was obvious that the cumulative height of AuNCs-Aptamer appeared to be roughly 4.5 nm, while the diameter of a local double helix RNA was estimated to be approximately 2 nm. It suggested that the height of AuNCs was approximately 2 nm, which was consistent with the result of TEM characterization. In general, the above results verified that

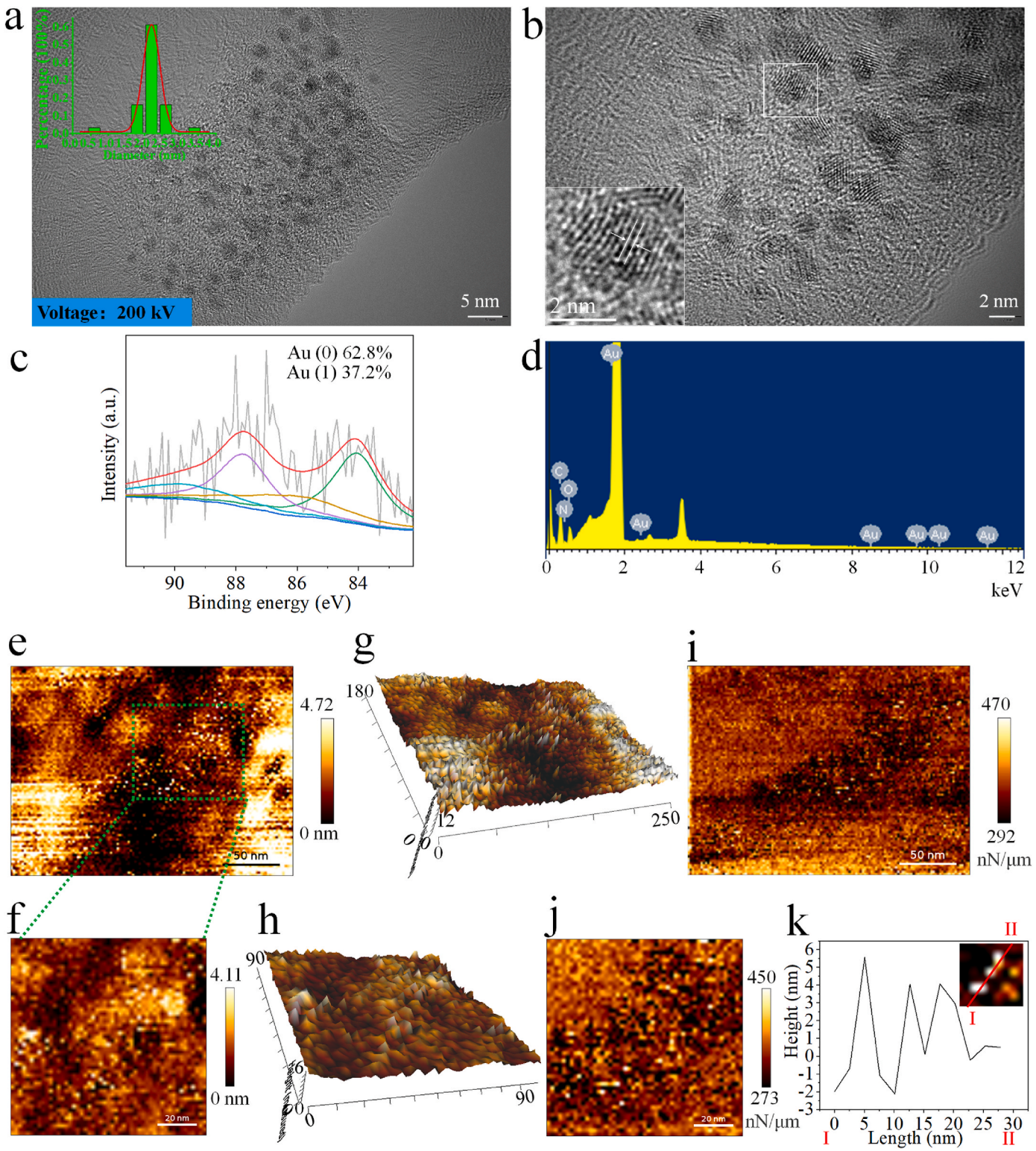

Fig. 2. The characterization of the extracted AuNCs-Aptamer. (a) TEM image and the diameter distribution histogram of AuNCs. The average particle size was 2.18 nm. (b) HR-TEM image. The lattice fringe spacing was 0.22 nm, corresponding to the Au (111) planes. XPS and EDS were respectively exhibited in (c) and (d). (e) The typical AFM images of the OSM-responsively self-assembled AuNCs-Aptamer in the damaged skin. The coordination precursor complexes of $HAuCl_4$ (1 mM) and aptamer (10 μM) were injected into the depilated dorsal skin. (f) The local enlarged image in (e). The bright areas represented AuNCs-Aptamer. The maximum superposition height of AuNCs-Aptamer was about 4.72 nm. (g) and (h) showed the three-dimensional model diagrams corresponding to (e) and (f), respectively. (i) and (j) were the rigidity diagrams corresponding to (e) and (f). (k) The height map of AuNCs-Aptamer along the marked red line (I→II) in the insert from (e). (For interpretation of the references to color in this figure legend, the reader is referred to the Web version of this article.)

AuNCs-Aptamer complexes were self-assembled successfully.

3.3. AuNCs-aptamer inhibiting hair follicle regeneration via negatively regulating the NFκB-mediated inflammatory response

In the OSM of damaged skin, the gold and anti-NFκB aptamer coordination precursors could form AuNCs-Aptamer. However, whether they could prevent the NFκB dimer efficiently and cell-specifically from binding to genomic DNA was unknown. Accordingly, we demonstrated at first that the anti-NFκB aptamer was delivered into damaged cells specifically through *in vitro* scratch injury assay. It was confirmed that there was an OSM in the damaged skin cells [100,101], and hereby we scratched JB6 cells to simulate the damage of skin cells. As shown in Fig. 3, the gold and Cy3-labeled anti-NFκB aptamer formed the coordination precursor complexes (Au + Cy3Apt) to facilitate the targeted uptake of the aptamer into the oxidative stress-damaged JB6 skin cells rather than the normal cells, and there was no significant uptake in the damaged or undamaged JB6 after the alone dose of the Cy3-labeled aptamer. This result was consistent with previous researches, which demonstrated inflammatory diseases and tumor development were involved in a large number of oxidative stress molecules (ROS and endogenous glutathione) [102–105] and that metal ions were tumor microenvironment-responsive to deliver functional nucleic acid molecules precisely into tumor cells with high oxidative stress by oxidative stress-responsively self-assembled AuNCs-DNA, AuNCs-miRNAs, AuNCs-shRNA and AuNCs&Fe-miRNA complexes [88–90,106]. As for the self-assembly mechanism, relevant processes were briefly summarized as follows: the coordination precursor complexes of $HAuCl_4$ and the nucleic acid were actively transported into the cell via endocytosis, Au^{+3} was reduced to $Au^{0/+1}$ using nucleic acid molecules as a template in the presence of intracellular antioxidants such as GSH and NADPH, and the self-assembled complexes of gold nanoclusters and nucleic acid formed. Reasonably, the plucking-induced skin micro-damage caused oxidative stress [22,23,107,108], phospholipid peroxidation, high membrane destabilization, the increased permeability of membrane [109] and the increase of total antioxidants [97–99], resulting in the targeted uptake and self-assembly of AuNCs-Aptamer complexes in oxidative stress-damaged cells.

In the canonical NFκB signal pathway, the nuclear translocation of the NFκB dimer (P50/P65) complexes activated the transcription of downstream inflammatory cytokines [110–116], and tumor necrosis factor alpha (TNF-α) was crucial to activate HFSCs and promote hair follicle regeneration after the hair plucking-induced damage [22,23,117,118]. Therefore, we next detected the expression level of TNF-α in the whole layer skin at the different time points after administration by ELISA to investigate if the aptamer could perform the corresponding function. The results indicated the expression level of TNF-α in the whole layer skin from Au, Apt and Au + Apt group mice gradually decreased respectively from the 1st to the 4th and 8th day after the hair plucking, and it remained stable in the PBS treated skin (Fig. 4a). Especially, on the 8th day after administration, the expression level of TNF-α in the whole layer skin from the Au + Apt treated mice was lowest among that in other three group skins. Furthermore, we investigated the expression level of two other pro-inflammatory factors interleukin-1 beta (IL1 beta) and cysteine-cysteine motif chemokine ligand 2 (CCL2) regulated by NFκB [118,119]and found that their expression patterns were similar to that of TNFa (Fig. 4b and c). Additionally, gold nanoclusters embodied the characterization of nano-enzymes that scavenged ROS, thereby relieving the inflammatory injury caused by ROS [120–128]. The production of catalase mimetic activity was most likely attributable to the presence of mixed valence gold (0 and + 1), catalyzing the reaction with hydrogen peroxide and superoxide. The particle size of gold nanoparticles had an obvious influence on their peroxidase-mimicking activity, and gold nanoclusters exhibited the

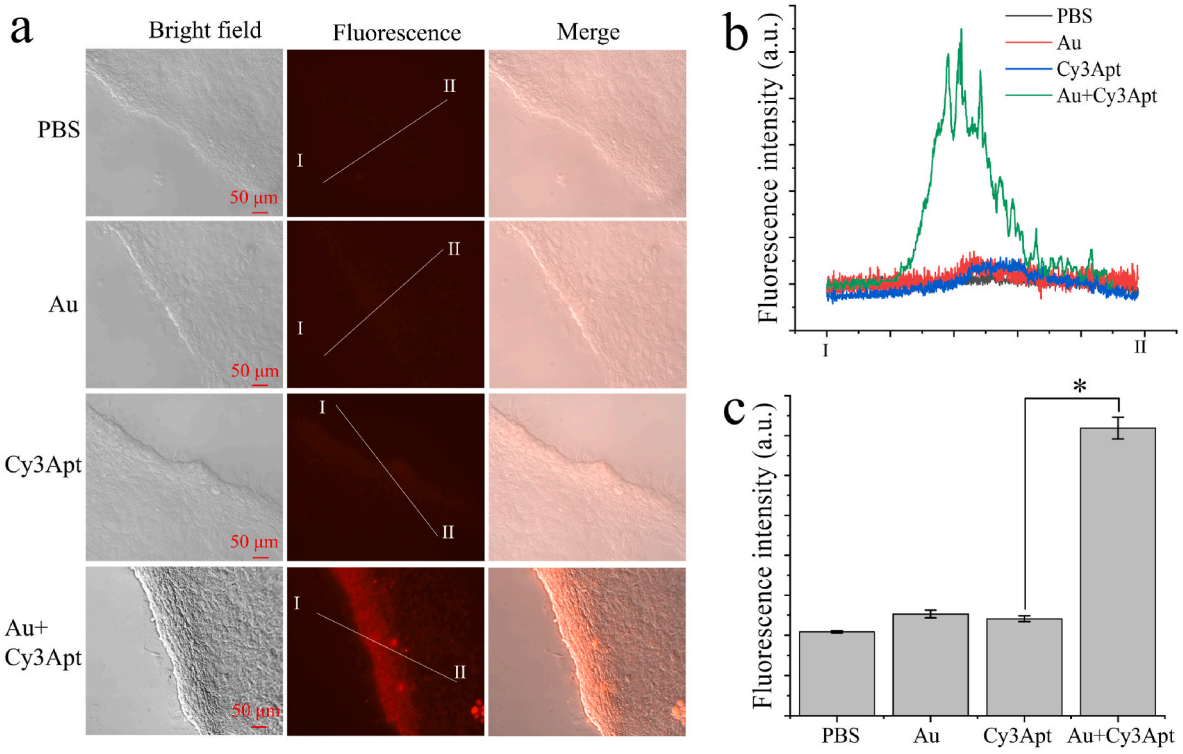

Fig. 3. The uptake of Cy3-labeled anti-NFκB aptamers in mechanically-damaged JB6 cells from the fluorescence microscope. (a) Cy3-labeled anti-NFκB aptamers were found in the injured cells around the scratch after administration of the $HAuCl_4$ and aptamer coordination precursor complexes, and there was no uptake of anti-NFkb aptamers after dose of the aptamer or $HAuCl_4$ alone. The merged pictures represented the overlap of the fluorescent and bright field. (b) The fluorescence intensity along the marked line (I→II) was analyzed by Image J software and (c) the corresponding fluorescence peak intensity statistics (*$P < 0.05$). The concentrations of $HAuCl_4$ and aptamers were 10 μM and 1 μM, respectively.

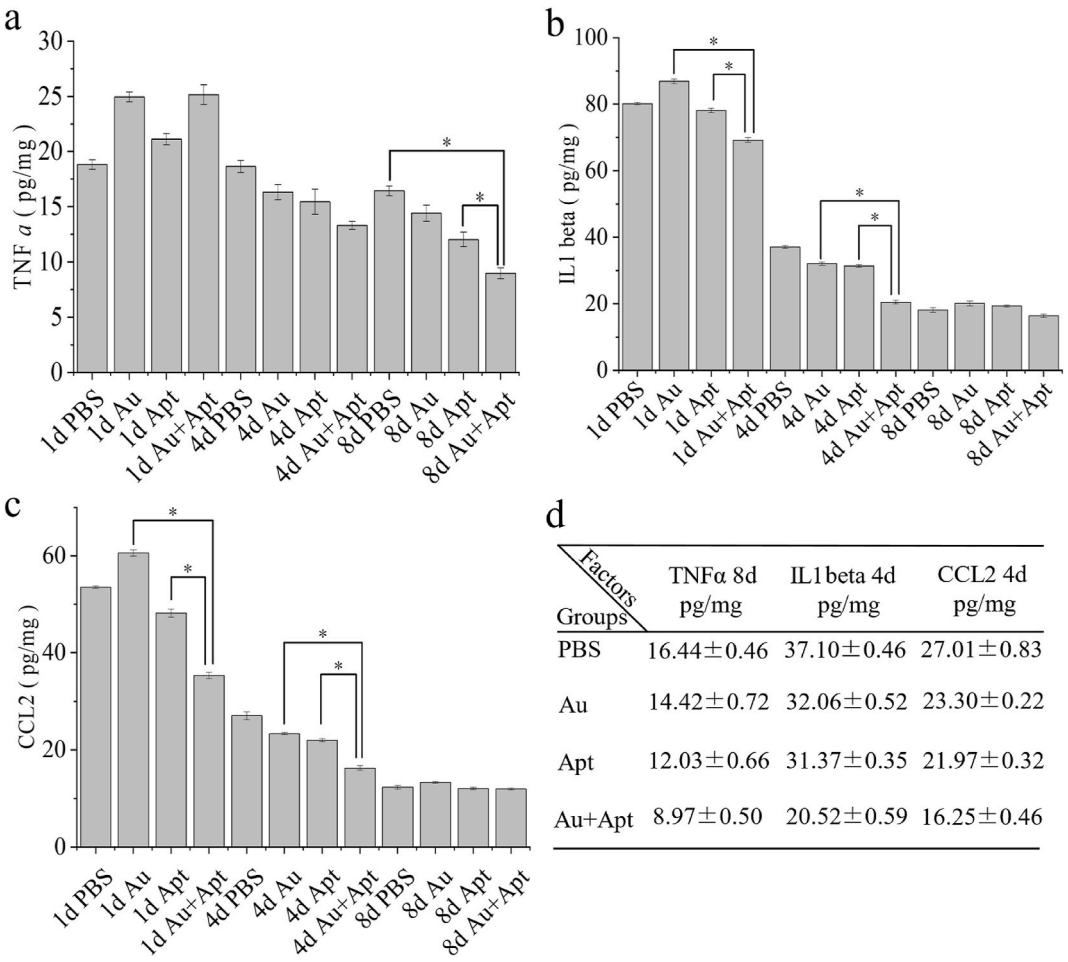

Groups \ Factors	TNFα 8d pg/mg	IL1beta 4d pg/mg	CCL2 4d pg/mg
PBS	16.44±0.46	37.10±0.46	27.01±0.83
Au	14.42±0.72	32.06±0.52	23.30±0.22
Apt	12.03±0.66	31.37±0.35	21.97±0.32
Au+Apt	8.97±0.50	20.52±0.59	16.25±0.46

Fig. 4. The expression level of (a) TNFα, (b) IL1 beta and (c) CCL2 in the whole layer skin respectively at the different time-points after administration by ELISA, and (d) the expression value of TNFα, IL1 beta and CCL2 corresponding to the 8^{th}, 4^{th} and 4^{th} day, denoting as mean ± standard deviation. The unit was pg/mg, representing the amount of the interested protein factor contained in total skin protein. (*P < 0.05).

highest activity at an optimized diameter of 1.9 nm [129,130], which was consistent with that of AuNCs (2.18 nm) in our self-assembled AuNCs-Aptamer. In short, AuNCs-Aptamer synergistically and negatively regulated NFκB-mediated inflammatory response signal pathway, resulting in inhibition of hair follicle regeneration.

Compared to the PBS group, the expression level of inflammatory factors (TNF-α, IL1 beta, and CCL2) did not change significantly in the Au group, which revealed that the nano-enzyme AuNCs could scavenge the excessive ROS [120–128] but not break the positive self-feedback loop with the NFκB as the core [118]. However, compared to the Au group, the expression level of inflammatory factors decreased significantly in the Au + Apt group, which demonstrated that the anti-NFκB aptamer in the self-assembled AuNCs-Aptamer complexes played a role in down-regulating the expression level of inflammatory factors. Furthermore, because the 29-nt aptamer against murine NFκB/p50 was adopted from Huang et al., characterizing the selective limitation on the targeted protein activity with negligible side effects, the mechanism by which the anti-p50 aptamer worked had been demonstrated to interact with the genomic DNA binding domain of NFκB and inhibit the ability of NFκB binding DNA and activating gene transcription [51,63,131,132], and it was not involved in IκBα phosphorylation and the p50/p65 nuclear translocation. In addition, **in** Fig. S8b in supporting information, there was no specific binding interaction between the aptamer and two kinds of activating protein-1, MAPK1/ERK2 mainly related to proliferation and differentiation and MAPK8/JNK1 primarily involved in oxidative stress response and inflammation, respectively. Accordingly, it excluded the possible cross-talk from MAPK/AP-1 pathways. To sum up, it was persuasive that AuNCs-Aptamer complexes inhibited the NFκB-mediated inflammatory response signaling pathway.

Finally, to further investigate the effect of AuNCs-Aptamer on the suppression of hair follicle regeneration, the paraffin sections of skin tissues on the 10^{th} day after the first administration were stained by immunofluorescence with the proliferation marker Ki67 and differentiation markers AE15/AE13. As evidenced by the arrows in Fig. 5a, Ki67 was strongly expressed in outer root sheath and hair matrix of the PBS, Au, Apt treated skin and the Au + Apt non-administrated site, and it was very weakly expressed in outer root sheath and second hair germ in the administrated site of the Au + Apt. AE15 was recommended for the detection of trichohyalin, which was produced in the inner root sheath and medulla of hair follicle [133,134]. AE13, pan-cytokeratin antibody, was recommended typically for the detection of the hair cortex keratin family [135,136]. As showed by the arrows in Fig. 5b and S11, AE15 was strongly expressed in the medulla and inner root sheath of the PBS, Au, Apt treated skin and the Au + Apt non-administrated site skin, and AE13 was strongly expressed in hair cortex of the PBS, Au, Apt treated skin and the Au + Apt non-administrated site skin. However, AE15 and AE13 were barely expressed in the administration site of the Au + Apt treated skin. Besides, the hair follicles in the dosed site of the Au + Apt treated skin were shortest in length among the anagen hair follicles of the PBS, Au, Apt treated skin and the Au + Apt non-administration site skin (Fig. S12). In the administration site of the Au + Apt treated skin, hair matrix did not encapsulate or partially encapsulated the dermal papilla, but it completely enveloped the dermal papilla in the PBS, Au, Apt treated skin and the Au + Apt non-administration site. These results

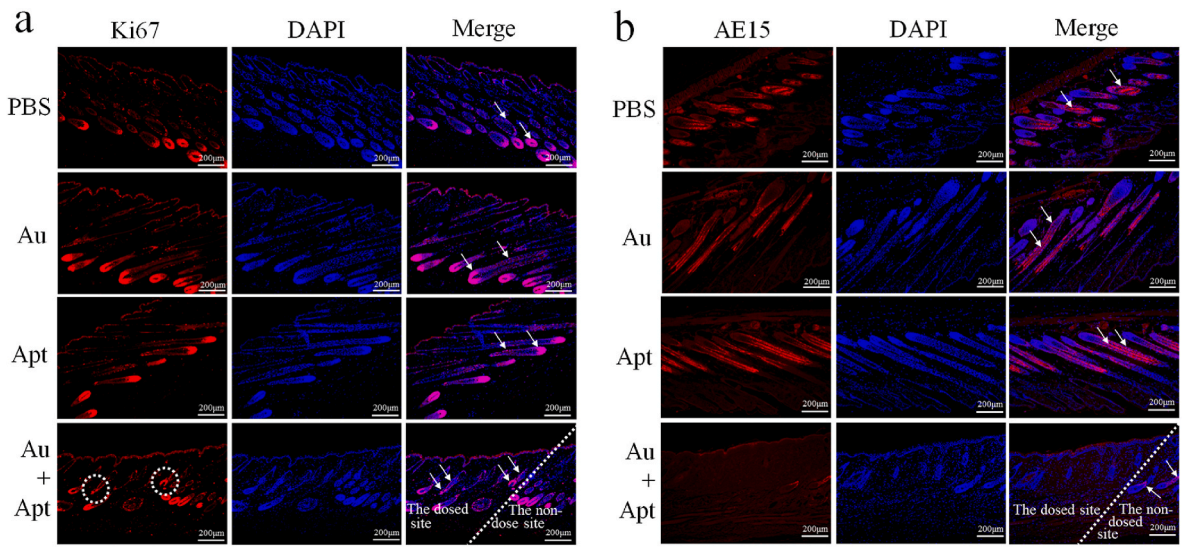

Fig. 5. The paraffin-embedded skin tissue section and immunofluorescence staining for (a) proliferation marker Ki67 and (b) differentiation marker AE15 to investigate the effects of AuNCs-Aptamer on proliferation and differentiation of hair follicle cells.

confirmed that the self-assembled AuNCs-Aptamer inhibited the proliferation and differentiation of hair follicle cells.

4. Conclusion

Since 2010, more and more researches on aptamer theranostics have been conducted [137], and there are dozens of aptamers used in clinical trials or as drugs [138,139]. Although the nucleic acid aptamer is a promising therapeutic against a wide variety of disorders due to its inherent advantages [51,52], there are some limitations, such as low cellular uptake and untoward side effects from high dose therapy [56,57,140,141]. Virus-based delivery carriers have biosafety concerns [53–55,76,142]. Nonvirus-based vectors transfection are challenged by their unsatisfactory efficiency, toxicity, and lack of specificity [143,144]. Gold nanoclusters have a wide range of biomedical theranostic applications because of its intrinsic characteristics [59–62], and *in vitro* synthesized gold nanoparticles (13 nm) serve as delivery carriers for nucleic acid transfection [145]. However, the biological toxicity and side effects are inevitable because of the relatively large diameter and the introduction of additional stabilizers and reductants in the process of synthesis [146,147]. The in-situ formed gold nanoclusters with a particle size below the renal clearance threshold (about 5.5 nm) was biosafe. In addition, many studies have reported $HAuCl_4$ precursors as the drug formulation were used for cancer imaging and treatment [89,90,148–150]. Thus, the in situ self-assembled AuNCs-aptamer as a delivery system has the remarkable advantages of avoiding high toxic transfection reagents and instability of *in vitro* synthesized nanoparticles. It is noted that this simple self-assembly approach not only resolves the targeting and safety of RNA aptamer delivery but also achieves effective inhibition of hair follicle regeneration. Hence, it opens up new opportunities for aptamer-based hypertrichosis therapy.

The hypertrichosis related to the skin damage is usually accompanied by the inflammation and the generation of ROS [10–12,14,15,24,30,32], which is an activator for hair follicle regeneration [18–21]. Summarily, our study manifested that OSM-responsively self-assembled AuNCs-Aptamer (Au^0 and Au^{+1}) exhibited the enhanced fluorescence imaging and the suppression of the hair follicle regeneration after administration of the aptamer and $HAuCl_4$ coordination precursors (Au^{+3}). At first, we confirmed the fluorescence enhancement and inhibiting the hair follicle regeneration only occurred in the Au + Apt treated skin. There was no obvious fluorescence and hair inhibition after administration of the $HAuCl_4$ or aptamer alone. Secondly, self-assembled AuNCs-Aptamer complexes were extracted from the skin and confirmed. The coordination precursor of Cy3-labeled anti-NFκB aptamer and $HAuCl_4$ facilitated the targeted uptake of the aptamer into the oxidative stress-damaged JB6 skin cells rather than the normal cells. In addition, ELISA for the inflammatory markers (TNF-α, IL1 beta and CCL2) and immunofluorescence staining for the proliferation and differentiation indicators (Ki67, AE13 and AE15) demonstrated the AuNCs-Aptamer inhibited the proliferation and differentiation of hair follicle cells via negatively regulating the NFκB-mediated inflammatory response signaling pathway. Finally, the analysis of hematology and HE staining of tissue section revealed the AuNCs-Aptamer had no toxic effect on the organism. Therefore, the self-assembled AuNCs-Aptamer is a targeted, safe and effective therapeutic for hypertrichosis involved in the skin inflammation and injury.

CRediT authorship contribution statement

Xiangdong Lai: Writing – original draft, Software, Methodology, Investigation, Formal analysis, Data curation, Conceptualization. **Xiaoyang Zhang:** Methodology, Investigation, Data curation. **Jiejuan Lai:** Formal analysis, Data curation. **Weiwei Zhao:** Investigation, Formal analysis. **Zhongquan Song:** Formal analysis, Data curation. **Yuanyuan Chen:** Investigation, Formal analysis. **Miraj Ud din:** Formal analysis. **Muhammad Faizan Munawer:** Formal analysis. **Hui Jiang:** Writing – review & editing, Data curation. **Xiaohui Liu:** Writing – review & editing, Data curation. **Xuemei Wang:** Writing – review & editing, Supervision, Resources, Project administration, Funding acquisition, Conceptualization.

Declaration of competing interest

The authors declare that they have no known competing financial interests or personal relationships that could have appeared to influence the work reported in this paper.

Acknowledgements

This work was supported by the National Natural Science Foundation of China (No. 82027806, 92461308, 82061148012, 82372220, 21974019), the National High-tech R&D Program and National Key Research & Development Program of China (2017YFA0205301), the National Key Research and Development Program of China (No.

2017YFA0205300) and the Primary Research & Development Plan of Jiangsu Province (No. BE2019716).

Appendix A. Supplementary data

Supplementary data to this article can be found online at https://doi.org/10.1016/j.mtbio.2025.101774.

Data availability

Data will be made available on request.

References

[1] F. Du, J. Li, S. Zhang, X. Zeng, J. Nie, Z. Li, Oxidative stress in hair follicle development and hair growth: signalling pathways, intervening mechanisms and potential of natural antioxidants, J. Cell Mol. Med. 28 (12) (2024) e18486.
[2] M.M. Welle, Basic principles of hair follicle structure, morphogenesis, and regeneration, Vet. Pathol. 60 (6) (2023) 732–747.
[3] M. Hosseini, K.R. Koehler, A. Shafiee, Biofabrication of human skin with its appendages, Adv. Healthc. Mater. 11 (22) (2022) 2201626.
[4] J. Lee, R. Böscke, P.-C. Tang, B.H. Hartman, S. Heller, K.R. Koehler, Hair follicle development in mouse pluripotent stem cell-derived skin organoids, Cell Rep. 22 (1) (2018) 242–254.
[5] Y. Lv, W. Yang, P.R. Kannan, H. Zhang, R. Zhang, R. Zhao, X. Kong, Materials-based hair follicle engineering: basic components and recent advances, Mater. Today Bio 29 (2024) 101303.
[6] K.S. Stewart, M.D. Abdusselamoglu, M.T. Tierney, A. Gola, Y.H. Hur, K.A. U. Gonzales, S. Yuan, A.R. Bonny, Y. Yang, N.R. Infarinato, C.J. Cowley, J. M. Levorse, H.A. Pasolli, S. Ghosh, C.V. Rothlin, E. Fuchs, Stem cells tightly regulate dead cell clearance to maintain tissue fitness, Nature 633 (8029) (2024) 407–416.
[7] L. Xiangyu, Z. Liang, H. Jing, Morphogenesis, growth cycle and molecular regulation of hair follicles, Front. Cell Dev. Biol. 10 (2022) 899095.
[8] S.A. Lee, K.N. Li, T. Tumbar, Stem cell-intrinsic mechanisms regulating adult hair follicle homeostasis, Exp. Dermatol. 30 (4) (2021) 430–447.
[9] L. Alonso, E. Fuchs, The hair cycle, J. Cell Sci. 119 (3) (2006) 391–393.
[10] C. Huang, L. Dong, B. Zhao, Y. Lu, S. Huang, Z. Yuan, G. Luo, Y. Xu, W. Qian, Anti-inflammatory hydrogel dressings and skin wound healing, Clin. Transl. Med. 12 (11) (2022) e1094.
[11] Y. Zhu, K. Wang, X. Jia, C. Fu, H. Yu, Y. Wang, Antioxidant peptides, the guardian of life from oxidative stress, Med. Res. Rev. 44 (1) (2024) 275–364.
[12] J. Md Jaffri, Reactive oxygen species and antioxidant system in selected skin disorders, Malays. J. Med. Sci. 30 (1) (2023) 7–20.
[13] M.R. Namazi, UV light may induce hypertrichosis through production of PGE2, Med. Hypotheses 68 (4) (2007) 917–918.
[14] P.E. Pizano, E.U. Suárez, Facial hypertrichosis, hyperpigmentation, and hepatosplenomegaly, Eur. J. Intern. Med. 92 (2021) 109–110.
[15] H. Sugino, M. Nakamura, Mild hypertrichosis in both upper arms around dupilumab injection sites, Eur. J. Dermatol. 31 (3) (2021) 420–421.
[16] M. Maleki, M.J. Yazdanpanah, H. Hamidi, L. Jokar, Evaluation of PUVA-induced skin side effects in patients referred to the imam reza hospital of mashhad in 2005-2007, Indian J. Dermatol. 59 (2) (2014) 209.
[17] F.H.J. Rampen, Hypertrichosis: a side-effect of PUVA therapy, Front. Cell Dev. Biol. 278 (1) (1985) 82–83.
[18] M.I. Calvo-Sánchez, S. Fernández-Martos, J.J. Montoya, J. Espada, Intrinsic activation of cell growth and differentiation in ex vivo cultured human hair follicles by a transient endogenous production of ROS, Sci. Rep. 9 (1) (2019) 4509.
[19] E. Carrasco, M.I. Calvo, A. Blázquez-Castro, D. Vecchio, A. Zamarrón, I.J.D. de Almeida, J.C. Stockert, M.R. Hamblin, Á. Juarranz, J. Espada, Photoactivation of ROS production in situ transiently activates cell proliferation in mouse skin and in the hair follicle stem cell niche promoting hair growth and wound healing, J. Invest. Dermatol. 135 (11) (2015) 2611–2622.
[20] M. Zheng, Y. Jang, N. Choi, D.Y. Kim, T.W. Han, J.H. Yeo, J. Lee, J.H. Sung, Hypoxia improves hair inductivity of dermal papilla cells via nuclear NADPH oxidase 4-mediated reactive oxygen species generation', Br. J. Dermatol. 181 (3) (2019) 523–534.
[21] H. Jin, Z. Zou, H. Chang, Q. Shen, L. Liu, D. Xing, Photobiomodulation therapy for hair regeneration: a synergetic activation of β-CATENIN in hair follicle stem cells by ROS and paracrine WNTs, Front. Cell Dev. Biol. 16 (6) (2021) 1568–1583.
[22] C.-C. Chen, L. Wang, Maksim V. Plikus, Ting X. Jiang, Philip J. Murray, R. Ramos, Christian F. Guerrero-Juarez, Michael W. Hughes, Oscar K. Lee, S. Shi, Randall B. Widelitz, Arthur D. Lander, Cheng M. Chuong, Organ-level quorum sensing directs regeneration in hair stem cell populations, Cell 161 (2) (2015) 277–290.
[23] X. Wang, H. Chen, R. Tian, Y. Zhang, M.S. Drutskaya, C. Wang, J. Ge, Z. Fan, D. Kong, X. Wang, T. Cai, Y. Zhou, J. Wang, J. Wang, S. Wang, Z. Qin, H. Jia, Y. Wu, J. Liu, S.A. Nedospasov, E.E. Tredget, M. Lin, J. Liu, Y. Jiang, Y. Wu, Macrophages induce AKT/β-catenin-dependent Lgr5(+) stem cell activation and hair follicle regeneration through TNF, Nat. Commun. 8 (2017) 14091.
[24] D. Saleh, S.N.S. Yarrarapu, C. Cook, Hypertrichosis, StatPearls, Treasure Island (FL), 2021.
[25] C. Erem, Update on idiopathic hirsutism: diagnosis and treatment, Acta Clin. Belg. 68 (4) (2013) 268–274.
[26] G.T. Tang, S. Zwickl, R. Sinclair, J.D. Zajac, A.S. Cheung, Effect of gender-affirming hormone therapy on hair growth: a systematic review of the literature, Clin. Exp. Dermatol. 48 (10) (2023) 1117–1127.
[27] M. Randolph, A. Tosti, Oral minoxidil treatment for hair loss: a review of efficacy and safety, J. Am. Acad. Dermatol. 84 (3) (2021) 737–746.
[28] J. Jimenez-Cauhe, D. Saceda-Corralo, R. Rodrigues-Barata, A. Hermosa-Gelbard, O.M. Moreno-Arrones, R. Gil-Redondo, D. Ortega-Quijano, D. Fernandez-Nieto, P. Jaen-Olasolo, S. Vaño-Galvan, Characterization and management of hypertrichosis induced by low-dose oral minoxidil in the treatment of hair loss, J. Am. Acad. Dermatol. 84 (1) (2021) 222–223.
[29] R.M. Trüeb, N. Caballero-Uribe, Minoxidil-induced hypertrichosis in a breastfed infant, J. Eur. Acad. Dermatol. Venereol. 36 (3) (2022) e224–e225.
[30] M. Kayani, E. Khalil, J. Sultan, F. Sagheer, Juvenile dermatomyositis with rare cutaneous manifestation: generalised hypertrichosis, J. Pak. Med. Assoc. 73 (7) (2023) 1539–1541.
[31] F.Z. Elfatoifi, S. Chiheb, P. Humbert, Hypertrichose infra-patellaire au cours d'une dermatomyosite chez l'adulte, Ann. Dermatol. Venereol. 144 (2) (2017) 161–162.
[32] M. Elosua-González, M. Campos-Domínguez, D. Bancalari, L. Noguera-Morel, A. Hernández-Martín, J. Huerta-Aragonés, A. Torrelo, Omeprazole-induced hypertrichosis in two children, Pediatr. Dermatol. 35 (4) (2018) e212–e214.
[33] M. Starace, S. Cedirian, L. Rapparini, F. Bruni, B.M. Piraccini, Vorasidenib-induced trichomegaly and hypertrichosis: a new side effect in a patient with diffuse astrocytoma, Dermatol. Ther. 14 (10) (2024) 2917–2921.
[34] D. Alexandris, N. Alevizopoulos, K. Palamaris, C. Gakiopoulou, S. Theocharis, Pinnae and facial hypertrichosis induced by cetuximab, J. Oncol. Pharm. Pract. 29 (3) (2023) 731–737.
[35] W. Hafsi, T. Badri, Hirsutism, StatPearls, Treasure Island (FL), 2021.
[36] A. Shrimal, S. Sardar, S. Roychoudhury, S. Sarkar, Long-pulsed Nd: YAG laser and intense pulse light-755 nm for idiopathic facial hirsutism: a comparative study, J. Cutan. Aesthet. Surg. 10 (1) (2017) 40–44.
[37] E.J. van Zuuren, Z. Fedorowicz, Interventions for hirsutism excluding laser and photoepilation therapy alone: abridged Cochrane systematic review including GRADE assessments, Br. J. Dermatol. 175 (1) (2016) 45–61.
[38] N. Somani, D. Turvy, Hirsutism: an evidence-based treatment update, Am. J. Clin. Dermatol. 15 (3) (2014) 247–266.
[39] R. Paparodis, A. Dunaif, The Hirsute woman: challenges in evaluation and management, Endocr, In Pract. 17 (5) (2011) 807–818.
[40] Y. Inoue, H. Nishioka, M. Inukai, Y. Shimizu, M. Kimura, H. Akita, T. Okumoto, What are the factors that induce paradoxical hypertrichosis after laser hair removal? Aesthet. Surg. J. 44 (5) (2024) NP347–NP353.
[41] D. Lizneva, L. Gavrilova-Jordan, W. Walker, R. Azziz, Androgen excess: investigations and management, Best Pract. Res. Clin. Obstet. Gynaecol. 37 (2016) 98–118.
[42] F. Jimenez, E. Poblet, A. Izeta, Reflections on how wound healing-promoting effects of the hair follicle can be translated into clinical practice, Exp. Dermatol. 24 (2) (2015) 91–94.
[43] D.M. Ansell, J.E. Kloepper, H.A. Thomason, R. Paus, M.J. Hardman, Exploring the "hair growth-wound healing connection": anagen phase promotes wound re-epithelialization, J. Invest. Dermatol. 131 (2) (2011) 518–528.
[44] C.L. Garcin, D.M. Ansell, The battle of the bulge: re-evaluating hair follicle stem cells in wound repair, Exp. Dermatol. 26 (2) (2017) 101–104.
[45] M.L. Martinez, E. Escario, E. Poblet, D. Sanchez, F.F. Buchon, A. Izeta, F. Jimenez, Hair follicle-containing punch grafts accelerate chronic ulcer healing: a randomized controlled trial, J. Am. Acad. Dermatol. 75 (5) (2016) 1007–1014.
[46] F. Heidari, A. Yari, H. Rasoolijazi, M. Soleimani, A. Dehpoor, N. Sajedi, S. Joulai Veijouye, M. Nobakht, Bulge hair follicle stem cells accelerate cutaneous wound healing in rats, Wounds 28 (4) (2016) 132–141.
[47] J.D. Fox, K.L. Baquerizo-Nole, F. Van Driessche, E. Yim, B. Nusbaum, F. Jimenez, R.S. Kirsner, Optimizing skin grafting using hair-derived skin grafts: the healing potential of hair follicle pluripotent stem cells, Wounds 28 (4) (2016) 109–111.
[48] K. Krieger, S.E. Millar, N. Mikuda, I. Krahn, J.E. Kloepper, M. Bertolini, C. Scheidereit, R. Paus, R. Schmidt-Ullrich, NF-κB participates in mouse hair cycle control and plays distinct roles in the various pelage hair follicle types, J. Invest. Dermatol. 138 (2) (2018) 256–264.
[49] S. Jeong, Y. Na, H.M. Nam, G.Y. Sung, Skin-on-a-chip strategies for human hair follicle regeneration, Exp. Dermatol. 32 (1) (2023) 13–23.
[50] V. Duheron, E. Hess, M. Duval, M. Decossas, B. Castaneda, J.E. Klöpper, L. Amoasii, J.-B. Barbaroux, I.R. Williams, H. Yagita, J. Penninger, Y. Choi, F. Lézot, R. Groves, R. Paus, C.G. Mueller, Receptor activator of NF-κB (RANK) stimulates the proliferation of epithelial cells of the epidermo-pilosebaceous unit, Proc. Natl. Acad. Sci. U. S. A. 108 (13) (2011) 5342–5347.
[51] M. Razlansari, S. Jafarinejad, A. rahdar, M. Shirvaliloo, R. Arshad, S. Fathi-Karkan, S. Mirinejad, S. Sargazi, R. Sheervalilou, N. Ajalli, S. Pandey, Development and classification of RNA aptamers for therapeutic purposes: an updated review with emphasis on cancer, Mol. Cell. Biochem. 478 (7) (2023) 1573–1598.
[52] J. Zhou, J. Rossi, Aptamers as targeted therapeutics: current potential and challenges, Nat. Rev. Drug Discov. 16 (3) (2017) 181–202.
[53] R. Chan, M. Gilbert, K.M. Thompson, H.N. Marsh, D.M. Epstein, P.S. Pendergrast, Co-expression of anti-NFκB RNA aptamers and siRNAs leads to maximal suppression of NFκB activity in mammalian cells, Nucleic Acids Res. 34 (5) (2006) e36-e36.

[54] D.L. DiGiusto, A. Krishnan, L. Li, H. Li, S. Li, A. Rao, S. Mi, P. Yam, S. Stinson, M. Kalos, J. Alvarnas, S.F. Lacey, J.-K. Yee, M. Li, L. Couture, D. Hsu, S.J. Forman, J.J. Rossi, J.A. Zaia, RNA-based gene therapy for HIV with lentiviral vector–modified CD34+ cells in patients undergoing transplantation for AIDS-related lymphoma, Sci. Transl. Med. 2 (36) (2010), 36ra43-36ra43.

[55] M.-J. Li, J. Kim, S. Li, J. Zaia, J.-K. Yee, J. Anderson, R. Akkina, J.J. Rossi, Long-term inhibition of HIV-1 infection in primary hematopoietic cells by lentiviral vector delivery of a triple combination of anti-HIV shRNA, anti-CCR5 ribozyme, and a nucleolar-localizing TAR decoy, Mol. Ther. 12 (5) (2005) 900–909.

[56] D. De Stefano, G. De Rosa, M.C. Maiuri, F. Ungaro, F. Quaglia, T. Iuvone, M. P. Cinelli, M.I. La Rotonda, R. Carnuccio, Oligonucleotide decoy to NF-κB slowly released from PLGA microspheres reduces chronic inflammation in rat, Pharmacol. Res. 60 (1) (2009) 33–40.

[57] C.H. Liu, J. Ren, P.K. Liu, Amphetamine manipulates monoamine oxidase-A level and behavior using theranostic aptamers of transcription factors AP-1/NF-kB, J. Biomed. Sci. 23 (1) (2016) 21.

[58] L. Berti, G.A. Burley, Nucleic acid and nucleotide-mediated synthesis of inorganic nanoparticles, Nat. Nanotechnol. 3 (2) (2008) 81–87.

[59] N. Kaur, R.N. Aditya, A. Singh, T.R. Kuo, Biomedical applications for gold nanoclusters: recent developments and future perspectives, Nanoscale Res. Lett. 13 (1) (2018) 302.

[60] Y. Zheng, L. Lai, W. Liu, H. Jiang, X. Wang, Recent advances in biomedical applications of fluorescent gold nanoclusters, Adv. Colloid Interface Sci. 242 (2017) 1–16.

[61] G. Zuber, E. Weiss, M. Chiper, Biocompatible gold nanoclusters: synthetic strategies and biomedical prospects, Nanotechnology 30 (35) (2019) 352001.

[62] A. Yahia-Ammar, D. Sierra, F. Mérola, N. Hildebrandt, X. Le Guével, Self-assembled gold nanoclusters for bright fluorescence imaging and enhanced drug delivery, ACS Nano 10 (2) (2016) 2591–2599.

[63] D.-B. Huang, D. Vu, L.A. Cassiday, J.M. Zimmerman, L.J. Maher, G. Ghosh, Crystal structure of NF-κB (p50)2 complexed to a high-affinity RNA aptamer, Proc. Natl. Acad. Sci. U. S. A. 100 (16) (2003) 9268–9273.

[64] F. Eckstein, Phosphorothioates, essential components of therapeutic oligonucleotides, Nucl. Acid Ther. 24 (6) (2014) 374–387.

[65] M. Flamme, L.K. McKenzie, I. Sarac, M. Hollenstein, Chemical methods for the modification of RNA, Methods 161 (2019) 64–82.

[66] D.E. Volk, G.L.R. Lokesh, Development of phosphorothioate DNA and DNA thioaptamers, Biomedicines 5 (3) (2017) 41.

[67] P. Guga, M. Boczkowska, M. Janicka, A. Maciaszek, B. Nawrot, S. Antoszczyk, W. J. Stec, Enhanced P-stereodependent stability of complexes formed by phosphorothioate oligonucleotides due to involvement of sulfur as strong hydrogen bond acceptor, Pure Appl. Chem. 78 (5) (2006) 993–1002.

[68] T.M. Peters-Clarke, Q. Quan, B.J. Anderson, W.M. McGee, E. Lohr, A.S. Hebert, M. S. Westphall, J.J. Coon, Phosphorothioate RNA analysis by NETD tandem mass spectrometry, Mol. Cell. Proteomics 23 (4) (2024) 100742.

[69] X. Lai, T. Liu, Z. Guo, Y. Wang, J. Xiao, Q. Xia, X. Liu, H. Jiang, X. Wang, In situ formed fluorescent gold nanoclusters inhibit hair follicle regeneration in oxidative stress microenvironment via suppressing NFκB signal pathway, Chin. Chem. Lett. 36 (2) (2024) 109762.

[70] P. Yang, P. Lu, J. Luo, L. Du, J. Feng, T. Cai, Y. Yuan, H. Cheng, H. Hu, Transient stimulation of TRPV4-expressing keratinocytes promotes hair follicle regeneration in mice, Br. J. Pharmacol. 177 (18) (2020) 4181–4192.

[71] S. Sharma, V. Bibhuti, Q.D. J, S. Bashar, H, Hassan, Injectable platelet-rich fibrin for treatment of female pattern hair loss, J. Cosmet. Laser Ther. 26 (1–4) (2024) 17–25.

[72] S.Y. An, H.-S. Kim, S.Y. Kim, S.Y. Van, H.J. Kim, J.-H. Lee, S.W. Han, I.K. Kwon, C.-K. Lee, S.H. Do, Y.-S. Hwang, Keratin-mediated hair growth and its underlying biological mechanism, Commun. Biol. 5 (1) (2022) 1270.

[73] D. Humzah, B. Molina, G. Salti, C. Cigni, G. Bellia, F. Grimolizzi, Intradermal injection of hybrid complexes of high- and low-molecular-weight hyaluronan: where do we stand and where are we headed in regenerative medicine? Int. J. Mol. Sci. 25 (6) (2024) 3216.

[74] J. Zhao, H. Lin, L. Wang, K. Guo, R. Jing, X. Li, Y. Chen, Z. Hu, S. Gao, N. Xu, Suppression of FGF5 and FGF18 expression by cholesterol-modified siRNAs promotes hair growth in mice, Front. Pharmacol. 12 (2021) 666860.

[75] I.J. Moon, H.K. Yoon, D. Kim, M.E. Choi, S.H. Han, J.H. Park, S.W. Hong, H. Cho, D.-K. Lee, C.H. Won, Efficacy of asymmetric siRNA targeting androgen receptors for the treatment of androgenetic alopecia, Mol. Pharm. 20 (1) (2023) 128–135.

[76] B. Zhao, J. Li, M. Liu, N. Yang, Z. Bao, X. Zhang, Y. Dai, J. Cai, Y. Chen, X. Wu, DNA methylation mediates lncRNA2919 regulation of hair follicle regeneration, Int. J. Mol. Sci. 23 (16) (2022) 9481.

[77] J. Wang, Y. Ma, T. Li, J. Li, X. Yang, G. Hua, G. Cai, H. Zhang, Z. Liu, K. Wu, X. Deng, MiR-199a-3p regulates the PTPRF/β-Catenin Axis in hair follicle development: insights into the pathogenic mechanism of alopecia areata, Int. J. Mol. Sci. 24 (24) (2023) 17632.

[78] L. Chen, Q. Yu, F. Guo, X. Wang, Z. Cai, Q. Zhou, Neurotensin counteracts hair growth inhibition induced by chronic restraint stress, Exp. Dermatol. 33 (1) (2024) e14990.

[79] Z. Jia, K. Tian, Y. Zhong, X. Wang, S. Gao, W. Xu, K. Li, L. Wu, Effectiveness of combination therapy of broadband light and intradermal injection of tranexamic acid in the treatment of chloasma, J. Cosmet. Dermatol. 22 (5) (2023) 1536–1544.

[80] A.K. Gupta, P.R. Shruthi, W. Tong, T. Mesbah, S. Michela, B.M, Piraccini, Systematic review of mesotherapy: a novel avenue for the treatment of hair loss, J. Dermatol. Treat. 34 (1) (2023) 2245084.

[81] K.-H. Yi, B. Lee, M.J. Kim, S.-H. Lee, I.J. Hidajat, T.S. Lim, H.M. Kim, J.-H. Kim, Observation on cadavers and through ultrasonography using a 2 mm needle length for intradermal injections, Skin Res. Technol. 29 (11) (2023) e13529.

[82] J. Wang, G. Liu, Imaging nano-bio interactions in the kidney: toward a better understanding of nanoparticle clearance, Angew. Chem.-Int. Edit. 57 (12) (2018) 3008–3010.

[83] W. Lu, S. Wei, H. Shi, X. Le, G. Yin, T. Chen, Progress in aggregation-induced emission-active fluorescent polymeric hydrogels, Aggregate 2 (3) (2021) e37.

[84] D. Bera, N. Goswami, Driving forces and routes for aggregation-induced emission-based highly luminescent metal nanocluster assembly, J. Phys. Chem. Lett. 12 (37) (2021) 9033–9046.

[85] A. Karami, M. Hasani, Methods to functionalize gold nanoparticles with tandem-phosphorothioate DNA: role of physicochemical properties of the phosphorothioate backbone in DNA adsorption to gold nanoparticles, Anal. Methods 15 (33) (2023) 4104–4113.

[86] C.M. Ritchie, K.R. Johnsen, J.R. Kiser, Y. Antoku, R.M. Dickson, J.T. Petty, Ag nanocluster formation using a cytosine oligonucleotide template, J. Phys. Chem. C 111 (1) (2007) 175–181.

[87] X. Zhang, C.Q. Sun, H. Hirao, Guanine binding to gold nanoparticles through nonbonding interactions, Phys. Chem. Chem. Phys. 15 (44) (2013) 19284–19292.

[88] Y. Wang, K. Huang, Z. Qin, J. Zeng, Y. Zhang, L. Yin, X. Liu, H. Jiang, X. Wang, Ultraprecise real-time monitoring of single cells in tumors in response to metal ion-mediated RNA delivery, ACS Appl. Mater. Interfaces 14 (33) (2022) 37291–37300.

[89] M. Wang, Y. Chen, W. Cai, H. Feng, T. Du, W. Liu, H. Jiang, A. Pasquarelli, Y. Weizmann, X. Wang, In situ self-assembling Au-DNA complexes for targeted cancer bioimaging and inhibition, Proc. Natl. Acad. Sci. U. S. A. 117 (1) (2020) 308–316.

[90] W. Cai, H. Feng, L. Yin, M. Wang, X. Jiang, Z. Qin, W. Liu, C. Li, H. Jiang, Y. Weizmann, X. Wang, Bio responsive self-assembly of Au-miRNAs for targeted cancer theranostics, EBioMedicine 54 (2020) 102740.

[91] A.V. Lakhin, V.Z. Tarantul, L.V. Gening, Aptamers: problems, solutions and prospects, Acta Naturae 5 (19) (2013) 34–43.

[92] N.C. Pagratis, C. Bell, Y.F. Chang, S. Jennings, T. Fitzwater, D. Jellinek, C. Dang, Potent 2′-amino-, and 2′-fluoro-2-deoxyribonucleotide rna inhibitors of keratinocyte growth factor, Nat. Biotechnol. 15 (1) (1997) 68–73.

[93] J.-P. Shaw, K. Kent, J. Bird, J. Fishback, B. Froehler, Modified deoxyoligonucleotides stable to exonuclease degradation in serum, Nucleic Acids Res. 19 (4) (1991) 747–750.

[94] J. Kim, N.M. El Zahar, M.G. Bartlett, In vitro metabolism of 2′-ribose unmodified and modified phosphorothioate oligonucleotide therapeutics using liquid chromatography mass spectrometry, Biomed. Chromatogr. 34 (7) (2020) e4839.

[95] M. Hyjek-Składanowska, T.A. Vickers, A. Napiórkowska, B.A. Anderson, M. Tanowitz, S.T. Crooke, X.-h. Liang, P.P. Seth, M. Nowotny, Origins of the increased affinity of phosphorothioate-modified therapeutic nucleic acids for proteins, J. Am. Chem. Soc. 142 (16) (2020) 7456–7468.

[96] N.D. Abeydeera, M. Egli, N. Cox, K. Mercier, J.N. Conde, P.S. Pallan, D. M. Mizurini, M. Sierant, F.-E. Hibti, T. Hassell, T. Wang, F.-W. Liu, H.-M. Liu, C. Martinez, A.K. Sood, T.P. Lybrand, C. Frydman, R.Q. Monteiro, R.H. Gomer, B. Nawrot, X. Yang, Evoking picomolar binding in RNA by a single phosphorodithioate linkage, Nucleic Acids Res. 44 (17) (2016) 8052–8064.

[97] A.A. Franco, R.S. Odom, T.A. Rando, Regulation of antioxidant enzyme gene expression in response to oxidative stress and during differentiation of mouse skeletal muscle, Free Radic. Biol. Med. 27 (9–10) (1999) 1122–1132.

[98] B. Poljsak, Strategies for reducing or preventing the generation of oxidative stress, Oxid. Med. Cell. Longev. 2011 (2011) 194586.

[99] T.A. Trinh, T.L. Nguyen, J. Kim, Lignin-based antioxidant hydrogel patch for the management of atopic dermatitis by mitigating oxidative stress in the skin, ACS Appl. Mater. Interfaces 16 (26) (2024) 33135–33148.

[100] X. Ji, J. Zhou, Z. Zhou, Z. Liu, L. Yan, Y. Li, H. Guo, W. Su, H. Wang, D. Ni, Recovering skin-nerve interaction by nanoscale metal-organic framework for diabetic ulcers healing, Bioact. Mater. 42 (2024) 112–123.

[101] D.K. Israni, N.R. Raghani, J. Soni, M. Shah, B.G. Prajapati, M.R. Chorawala, S. Mangmool, S. Singh, C. Chittasupho, Harnessing cannabis sativa oil for enhanced skin wound healing: the role of reactive oxygen species regulation, Pharmaceutics 16 (10) (2024) 1277.

[102] Z. Kang, C. Wang, Y. Tong, Y. Li, Y. Gao, S. Hou, M. Hao, X. Han, B. Wang, Q. Wang, C. Zhang, Novel nonsecosteroidal vitamin D receptor modulator combined with gemcitabine enhances pancreatic cancer therapy through remodeling of the tumor microenvironment, J. Med. Chem. 64 (1) (2021) 629–643.

[103] L. Al-Akra, D.-H. Bae, L.Y.W. Leck, D.R. Richardson, P.J. Jansson, The biochemical and molecular mechanisms involved in the role of tumor micro-environment stress in development of drug resistance, Biochim. Biophys. Acta-Gen. Subj. 1863 (9) (2019) 1390–1397.

[104] F.Q. Schafer, G.R. Buettner, Redox environment of the cell as viewed through the redox state of the glutathione disulfide/glutathione couple, Free Radic. Biol. Med. 30 (11) (2001) 1191–1212.

[105] E.S. Lee, Z. Gao, Y.H. Bae, Recent progress in tumor pH targeting nanotechnology, J. Control. Release 132 (3) (2008) 164–170.

[106] W. Cai, L. Yin, H. Jiang, Y. Weizmann, X. Wang, Intelligent bio-responsive fluorescent Au–shRNA complexes for regulated autophagy and effective cancer bioimaging and therapeutics, Biosensors-Basel 11 (11) (2021) 425.

[107] D. Gay, O. Kwon, Z. Zhang, M. Spata, M.V. Plikus, P.D. Holler, M. Ito, Z. Yang, E. Treffeisen, C.D. Kim, A. Nace, X. Zhang, S. Baratono, F. Wang, D.M. Ornitz, S.

E. Millar, G. Cotsarelis, Fgf9 from dermal γδ T cells induces hair follicle neogenesis after wounding, Nat. Med. 19 (7) (2013) 916–923.
[108] N. Ali, B. Zirak, R.S. Rodriguez, M.L. Pauli, H.A. Truong, K. Lai, R. Ahn, K. Corbin, M.M. Lowe, T.C. Scharschmidt, K. Taravati, M.R. Tan, R.R. Ricardo-Gonzalez, A. Nosbaum, M. Bertolini, W. Liao, F.O. Nestle, R. Paus, G. Cotsarelis, A.K. Abbas, M.D. Rosenblum, Regulatory T cells in skin facilitate epithelial stem cell differentiation, Cell 169 (6) (2017) 1119–1129.e11.
[109] A. Gęgotek, K. Bielawska, M. Biernacki, I. Dobrzyńska, E. Skrzydlewska, Time-dependent effect of rutin on skin fibroblasts membrane disruption following UV radiation, Redox Biol. 12 (2017) 733–744.
[110] A. Oeckinghaus, S. Ghosh, The NF-kappaB family of transcription factors and its regulation, Cold Spring Harb. Perspect. Biol. 1 (4) (2009) a000034.
[111] K. Taniguchi, M. Karin, NF-κB, inflammation, immunity and cancer: coming of age, Nat. Rev. Immunol. 18 (5) (2018) 309–324.
[112] S. Prasad, V. Kumar, C. Singh, A. Singh, Crosstalk between phytochemicals and inflammatory signaling pathways, Inflammopharmacology 31 (3) (2023) 1117–1147.
[113] W. Sun, Y. Gao, X. Yu, Y. Yuan, J. Yi, Z. Zhang, Y. Cheng, Y. Li, X. Peng, X. Cha, 'Psoriasis 1' reduces psoriasis-like skin inflammation by inhibiting the VDR-mediated nuclear NF-κB and STAT signaling pathways, Mol. Med. Rep. 18 (3) (2018) 2733–2743.
[114] M.S. Hayden, S. Ghosh, Shared principles in NF-kappaB signaling, Cell 132 (3) (2008) 344–362.
[115] P. Viatour, M.P. Merville, V. Bours, A. Chariot, Phosphorylation of NF-kappaB and IkappaB proteins: implications in cancer and inflammation, Trends Biochem. Sci. 30 (1) (2005) 43–52.
[116] J. Zhang, J. Zhu, X. Chen, H. Xia, L. Yang, E3 ubiquitin ligase Trim33 ubiquitylates Annexin A2 to promote NF-κB induced skin inflammation in psoriasis, J. Dermatol. Sci. 107 (3) (2022) 160–168.
[117] M. Yusupova, R. Ankawa, Y. Yosefzon, D. Meiri, I. Bachelet, Y. Fuchs, Apoptotic dysregulation mediates stem cell competition and tissue regeneration, Nat. Commun. 14 (1) (2023) 7547.
[118] N. Kordulewska, J. Topa, A. Cieślińska, B. Jarmołowska, Osthole regulates secretion of pro-inflammatory cytokines and expression of TLR2 and NF-κB in normal human keratinocytes and fibroblasts, J. Inflamm. Res. 15 (2022) 1501–1519.
[119] X. Guo, W. Wang, L. Lin, J. Shan, J. Zhu, S. Ning, H. Li, X. Wang, D. Lu, MnGA with multiple enzyme-like properties for acute wound healing by reducing oxidative stress and modulating signaling pathways, Mater, Today Bio 30 (2025) 101435.
[120] F. Tian, S. Zhang, M. Wang, Y. Yan, Y. Cao, Y. Wang, K. Fan, H. Wang, J. Zhang, X.-D. Zhang, Clinical grade fibroin sutures with bioactive gold clusters enhance surgical wound healing via inflammation modulation, ACS Appl. Mater. Interfaces 16 (41) (2024) 55097–55106.
[121] J. Ding, M. Zhao, Y. Li, K. Zhang, H. Chen, X. Hu, L. Li, Y. Su, X. Yuan, Z. Lin, Atomically precise gold nanoclusters as ROS-scavenging clusterzymes to treat high-fat diet-induced obesity, Chem. Eng. J. 496 (2024) 153726.
[122] Y.-S. Borghei, S. Hosseinkhani, Cell membrane-coated AuNPs as a new biomimetic platform for ROS scavenger provides cytoprotection from apoptosis induced by oxidative stress, Part. Part. Syst. Charact. 40 (6) (2023) 2300006.
[123] J. Lou-Franco, B. Das, C. Elliott, C. Cao, Gold nanozymes: from concept to biomedical applications, Nano-Micro Lett. 13 (1) (2020) 10.
[124] Q. Dan, Z. Yuan, S. Zheng, H. Ma, W. Luo, L. Zhang, N. Su, D. Hu, Z. Sheng, Y. Li, Gold nanoclusters-based NIR-II photosensitizers with catalase-like activity for boosted photodynamic therapy, Pharmaceutics 14 (8) (2022) 1645.
[125] R.A. Pinho, D.P.S. Haupenthal, P.E. Fauser, A. Thirupathi, P.C.L. Silveira, Gold nanoparticle-based therapy for muscle inflammation and oxidative stress, J. Inflamm. Res. 15 (2022) 3219–3234.
[126] A.P. Muller, G.K. Ferreira, A.J. Pires, G. de Bem Silveira, D.L. de Souza, J. A. Brandolfi, C.T. de Souza, M.M.S. Paula, P.C.L. Silveira, Gold nanoparticles prevent cognitive deficits, oxidative stress and inflammation in a rat model of sporadic dementia of Alzheimer's type, Mater. Sci. Eng. C Mater. Biol. Appl. 77 (2017) 476–483.
[127] S. Huang, H. Xiang, J. Lv, Y. Guo, L. Xu, Propelling gold nanozymes: catalytic activity and biosensing applications, Anal. Bioanal. Chem. 416 (27) (2024) 5915–5932.
[128] J. Gao, Y. Zhou, G. Xu, Z. Wei, L. Ding, W. Zhang, Y. Huang, Hybrid hydrogels containing gradients in gold nanoparticles for localized delivery of mesenchymal stem cells and enhanced nerve tissues remodeling in vivo, Mater, Today Bio 30 (2025) 101411.
[129] M. Kalantari, T. Ghosh, Y. Liu, J. Zhang, J. Zou, C. Lei, C. Yu, Highly thiolated dendritic mesoporous silica nanoparticles with high-content gold as nanozymes: the nano-gold size matters, ACS Appl. Mater. Interfaces 11 (14) (2019) 13264–13272.
[130] D. Zhao, X. Huang, Y. Tian, J. Zou, F. Wang, X. Chen, Fluorescence imaging-incorporated transcriptome study of glutathione depletion-enhanced ferroptosis therapy via targeting gold nanoclusters, ACS Appl. Mater. Interfaces 15 (5) (2023) 6385–6396.
[131] O. Rabal, F. Pastor, H. Villanueva, M.M. Soldevilla, S. Hervas-Stubbs, J. Oyarzabal, In silico aptamer docking studies: from a retrospective validation to a prospective case Study'TIM3 aptamers binding, Mol. Ther.-Nucl. Acids 5 (2016) e376.
[132] G. Ghosh, G.V. Duyne, S. Ghosh, P.B. Sigler, Structure of NF-κB p50 homodimer bound to a κB site, Nature 373 (6512) (1995) 303–310.
[133] I. Cohen, D. Zhao, C. Bar, V.J. Valdes, K.L. Dauber-Decker, M.B. Nguyen, M. Nakayama, M. Rendl, W.A. Bickmore, H. Koseki, D. Zheng, E. Ezhkova, PRC1 fine-tunes gene repression and activation to safeguard skin development and stem cell specification, Cell Stem Cell 22 (5) (2018) 726–739.e7.
[134] H. Yang, R.C. Adam, Y. Ge, Z.L. Hua, E. Fuchs, Epithelial-Mesenchymal micro-niches govern stem cell lineage choices, Cell 169 (3) (2017) 483–496.e13.
[135] B. Lloyd-Lewis, F. Gobbo, M. Perkins, G. Jacquemin, M. Huyghe, M.M. Faraldo, S. Fre, In vivo imaging of mammary epithelial cell dynamics in response to lineage-biased Wnt/β-catenin activation, Cell Rep. 38 (10) (2022) 110461.
[136] M. Fernandez-Guerrero, N. Yakushiji-Kaminatsui, L. Lopez-Delisle, S. Zdral, F. Darbellay, R. Perez-Gomez, C.C. Bolt, M.A. Sanchez-Martin, D. Duboule, M. A. Ros, Mammalian-specific ectodermal enhancers control the expression of Hoxc genes in developing nails and hair follicles, Proc. Natl. Acad. Sci. Belarus-Agrar. Ser. 117 (48) (2020) 30509–30519.
[137] L. Bohrmann, T. Burghardt, C. Haynes, K. Saatchi, U.O. Häfeli, Aptamers used for molecular imaging and theranostics - recent developments, Theranostics 12 (9) (2022) 4010–4050.
[138] N. Zhang, Z. Chen, D. Liu, H. Jiang, Z.-K. Zhang, A. Lu, B.-T. Zhang, Y. Yu, G. Zhang, Structural biology for the molecular insight between aptamers and target proteins, Int. J. Mol. Sci. 22 (8) (2021) 4093.
[139] F. Radom, P.M. Jurek, M.P. Mazurek, J. Otlewski, F. Jeleń, Aptamers: molecules of great potential, Biotechnol. Adv. 31 (8) (2013) 1260–1274.
[140] D. Xu, Z. Hu, J. Su, F. Wu, W. Yuan, Micro and nanotechnology for intracellular delivery therapy protein, Nano-Micro Lett. 4 (2) (2012) 118–123.
[141] N.S. Gandhi, R.K. Tekade, M.B. Chougule, Nanocarrier mediated delivery of siRNA/miRNA in combination with chemotherapeutic agents for cancer therapy: current progress and advances, J. Control. Release 194 (2014) 238–256.
[142] K.-m. Choi, S.-H. Choi, H. Jeon, I.-S. Kim, H.J. Ahn, Chimeric capsid protein as a nanocarrier for siRNA delivery: stability and cellular uptake of encapsulated siRNA, ACS Nano 5 (11) (2011) 8690–8699.
[143] H. Ledford, Drug giants turn their backs on RNA interference, Nature 468 (7323) (2010), 487-487.
[144] H.M. Jan, M.F. Wei, C.L. Peng, S.J. Lin, P.S. Lai, M.J. Shieh, The use of polyethylenimine–DNA to topically deliver hTERT to promote hair growth, Gene Ther. 19 (1) (2012) 86–93.
[145] A. Ekin, O.F. Karatas, M. Culha, M. Ozen, Designing a gold nanoparticle-based nanocarrier for microRNA transfection into the prostate and breast cancer cells, J. Gene, Med 16 (11–12) (2014) 331–335.
[146] H.V. Nguyen, H.V. Nguyen, V.M. Phan, B.J. Park, T.S. Seo, Serially diluting centrifugal microfluidics for high-throughput gold nanoparticle synthesis using an automated and portable workstation, Chem. Eng. J. 452 (2023) 139044.
[147] S.E. Lohse, J.R. Eller, S.T. Sivapalan, M.R. Plews, C.J. Murphy, A simple millifluidic benchtop reactor system for the high-throughput synthesis and functionalization of gold nanoparticles with different sizes and shapes, ACS Nano 7 (5) (2013) 4135–4150.
[148] C. Zhao, T. Du, F.u. Rehman, L. Lai, X. Liu, X. Jiang, X. Li, Y. Chen, H. Zhang, Y. Sun, S. Luo, H. Jiang, M. Selke, X. Wang, Biosynthesized gold nanoclusters and iron complexes as scaffolds for multimodal cancer bioimaging, Small 12 (45) (2016) 6255–6265.
[149] H. Xiong, J. Ye, M. Wang, Y. Wang, X. Liu, H. Jiang, X. Wang, In-situ bio-assembled specific Au NCs-Aptamer-Pyro conjugates nanoprobe for tumor imaging and mitochondria-targeted photodynamic therapy, Biosens. Bioelectron. 218 (2022) 114763.
[150] W. Mi, S. Tang, S. Guo, H. Li, N. Shao, In situ synthesis of red fluorescent gold nanoclusters with enzyme-like activity for oxidative stress amplification in chemodynamic therapy, Chin. Chem. Lett. 33 (3) (2022) 1331–1336.
[151] W. Zhao, F. Gonzaga, Y. Li, M.A. Brook, Highly Stabilized Nucleotide-Capped Small Gold Nanoparticles with Tunable Size, Adv. Mater. 19 (13) (2007) 1766–1771.